

# Halide Perovskite Stabilized in a Photoelectrochemical Environment by Impermeable Single Crystal TiO<sub>2</sub> for Semi-artificial Photosynthesis

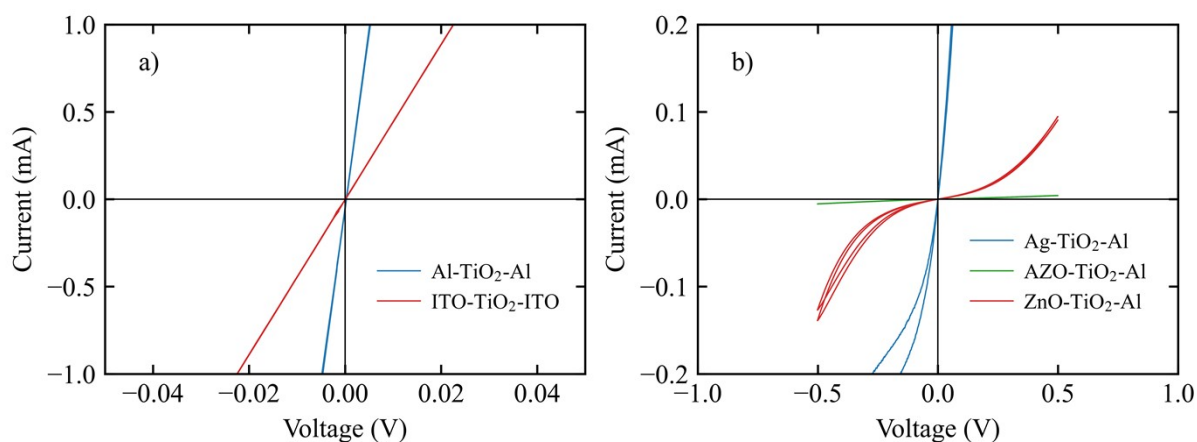


Figure S1. The  $I$ - $V$  measurements on TiO<sub>2</sub> crystals with electrical contacts on their front and backsides. The measurements showed that Al and Indium-doped SnO<sub>2</sub> (ITO) provide ohmic contacts, while Ag, ZnO, and Al-doped ZnO (AZO) exhibit rectifying contacts. The contact materials were deposited using a thermal evaporator (Al, Ag), e-beam evaporator (ZnO, AZO), or sputter (ITO) and Ag paste was applied on the contacts for the  $I$ - $V$  measurements.

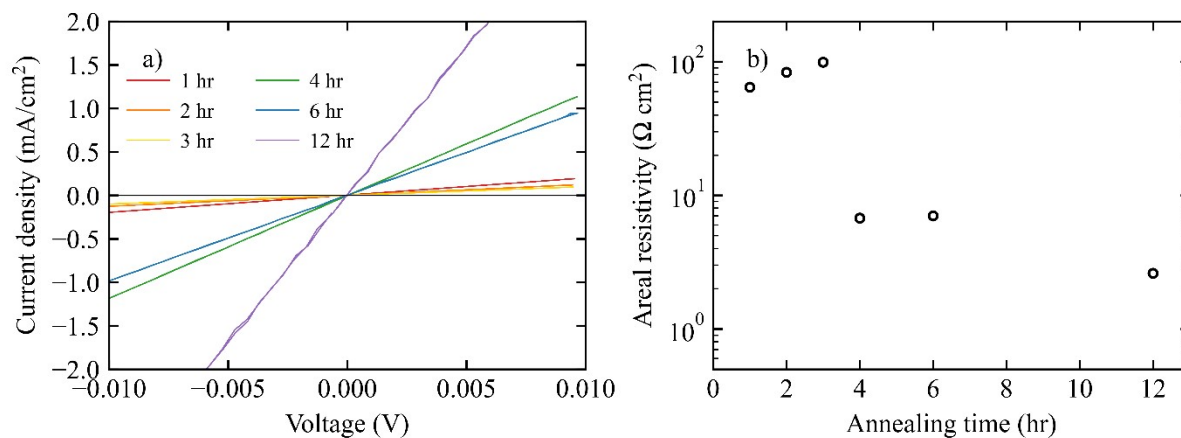


Figure S2. a) The  $I$ - $V$  measurements and b) the areal resistivity of a TiO<sub>2</sub> crystal (200 μm) sandwiched between two Al contacts depending on the annealing time.

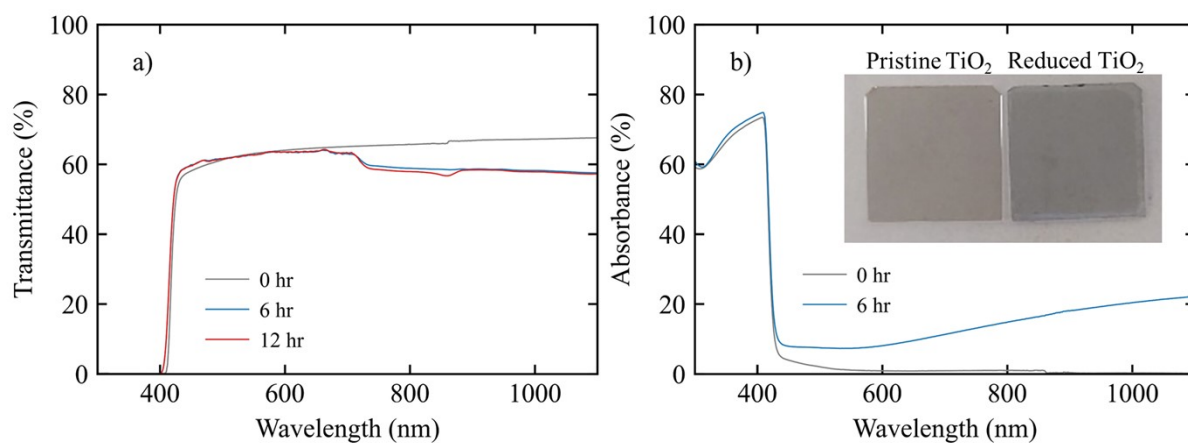


Figure S3. The a) transmittance and b) absorbance of  $\text{TiO}_2$  crystals (500  $\mu\text{m}$ ) depending on the annealing time.

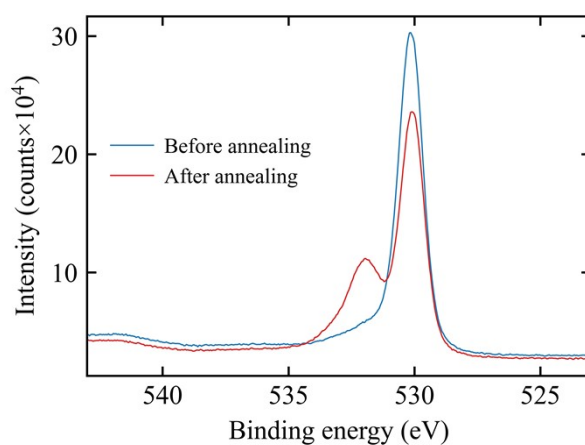


Figure S4. The XPS measurements on  $\text{O}1\text{s}$  orbitals of the single crystal  $\text{TiO}_2$  before and after thermal annealing for 6 hours. The secondary  $\text{O}1\text{s}$  peak appeared after the thermal annealing due to the oxygen defects generated during the thermal reduction.

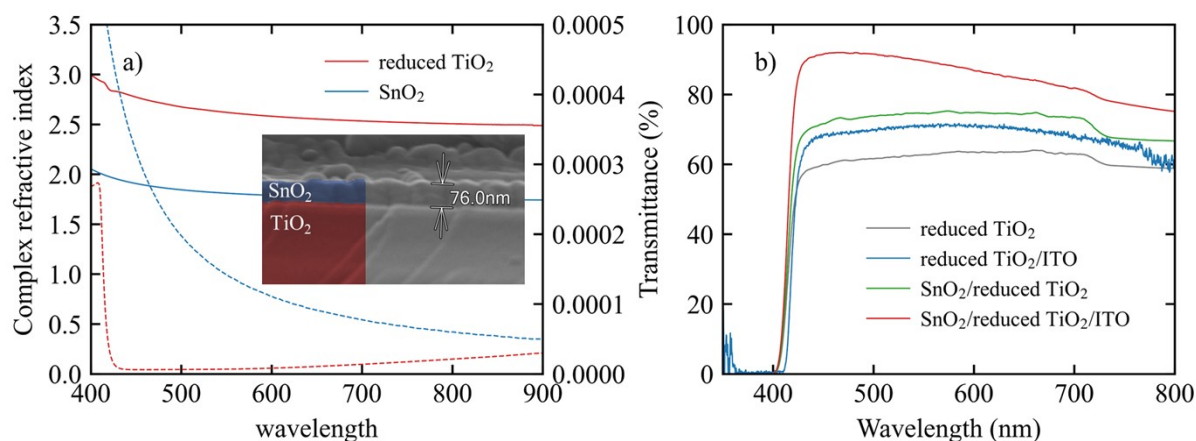


Figure S5. a) The real part (solid line) and the imaginary part (dashed line) of the complex refractive indices of TiO<sub>2</sub> and SnO<sub>2</sub>, which are derived from UV-VIS spectra of TiO<sub>2</sub> (Figure S5) and ellipsometry on SnO<sub>2</sub>. The inset SEM image shows the SnO<sub>2</sub> thin film coated on the TiO<sub>2</sub> crystal. b) The optical transmittances of TiO<sub>2</sub> crystal with or without SnO<sub>2</sub> anti-reflection coating or ITO contact.

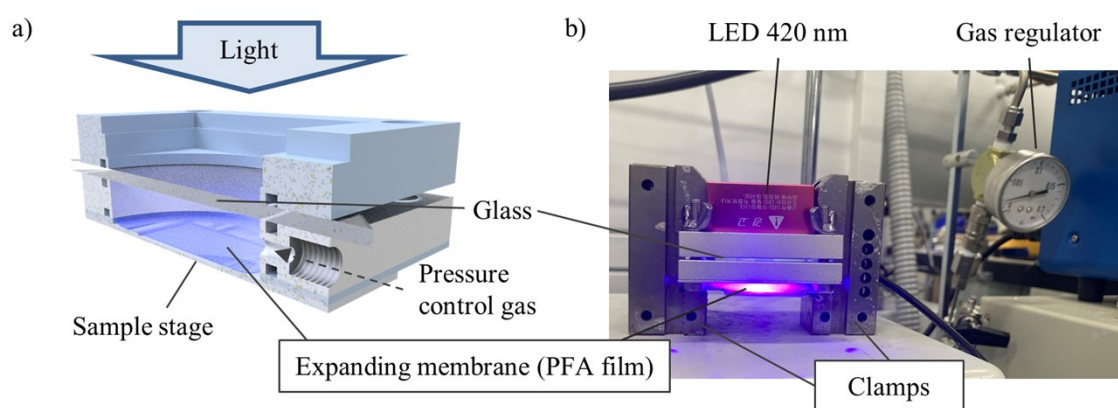


Figure S6. a) Schematic diagram and b) photograph of the pressurized curing setup (TiO<sub>2</sub> crystal and halide perovskite samples are not shown). The stack of TiO<sub>2</sub>, TCA, and halide perovskite is placed on the sample stage and in contact with the outer side of the expanding membrane. The pressure pressing the stack is equivalent to the N<sub>2</sub> gas filling the chamber. The pressure of N<sub>2</sub> gas is controlled by the gas regulator (0-0.2 MPa).

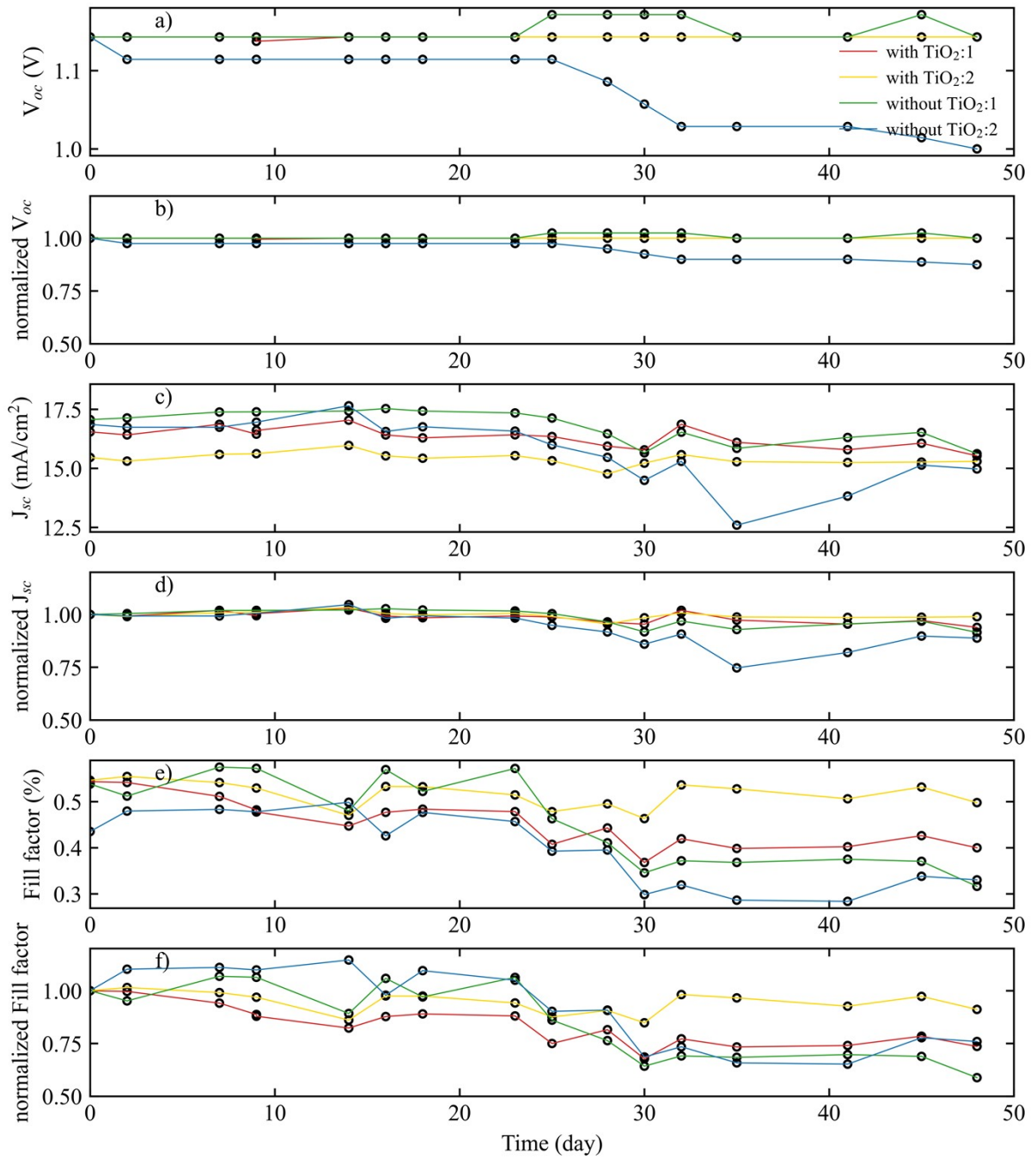


Figure S7. The stability tests on halide perovskite PV cells with p-i-n structure with or without  $\text{TiO}_2$  protection layer (2 cells for each). We carried out dry I-V measurements to characterize a) open-circuit voltage ( $V_{oc}$ ), b)  $V_{oc}$  normalized by the initial value, c) short-circuit current density ( $J_{sc}$ ), d)  $J_{sc}$  normalized by its initial value, e) fill factor (FF), and f) FF normalized by its initial value. The PV cells were kept in a vacuum chamber for the first 25 days and in air for the rest of the period. The stability tests show that the halide perovskite film is stable for more than 50 days and the encapsulation process using the  $\text{TiO}_2$  protection layer and TCA did not cause adverse effects on the stability of the halide perovskite film.

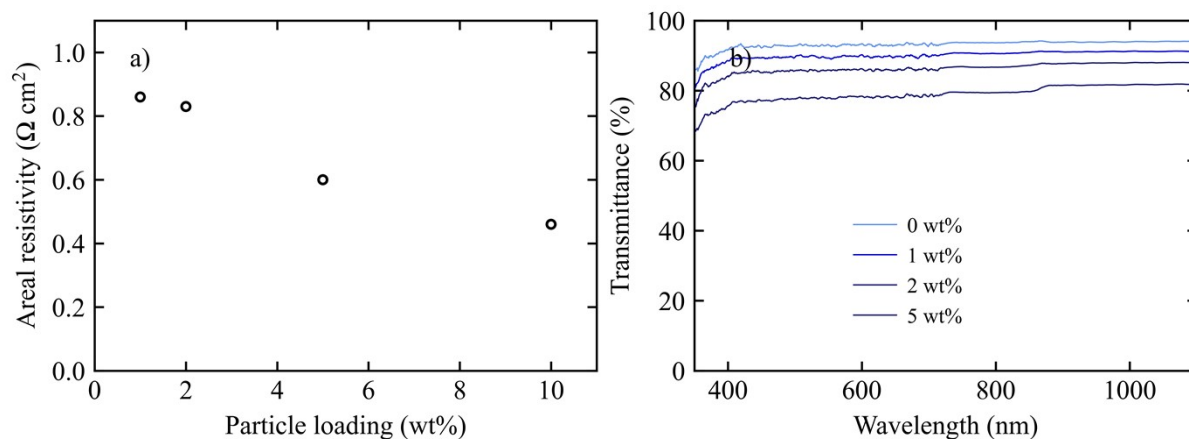


Figure S8. a) areal conductivity of TCA sandwiched between two stainless steel plates (20 mm×20 mm) and b) The transmittance of TCA sandwiched between two quartz substrates (25 mm×25 mm).

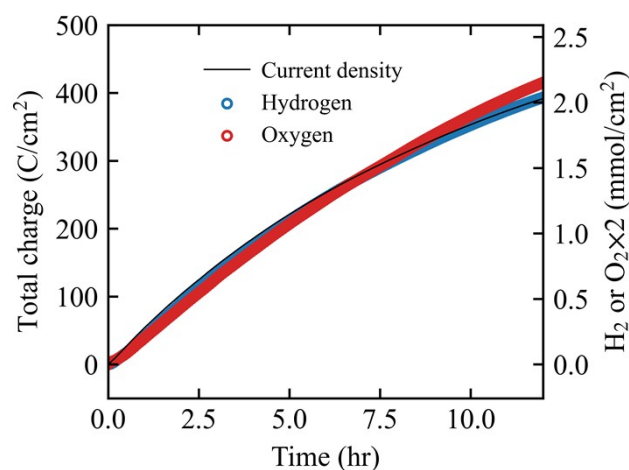


Figure S9. The gas chromatography measurement on the catalysts for HER and OER showing Faraday efficiency close to 100 %.

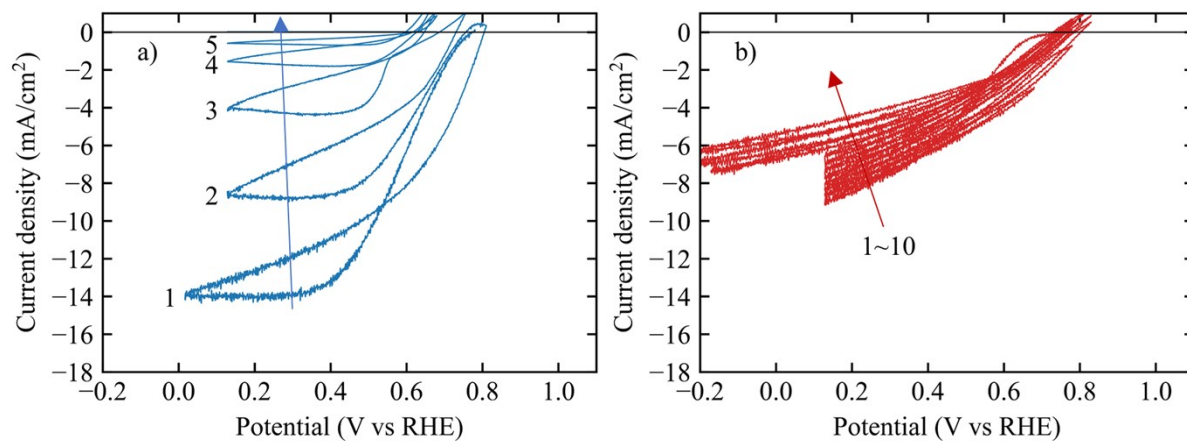


Figure S10. The cyclic voltammetry from halide perovskite photocathode a) without  $\text{TiO}_2$  protection

layer (Pt catalyst deposited on top of the ITO electrode over the *p-i-n* halide perovskite) and b) with a TiO<sub>2</sub> thin film (100 nm) protection layer and Pt catalyst deposited by an e-beam evaporator. Both devices exhibited immediate loss in the photovoltage and poor stability over the several cycles of the cyclic voltammetry.

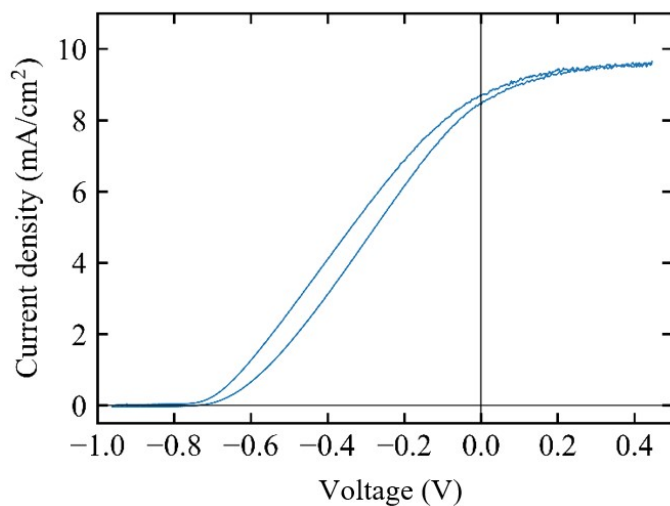


Figure S11. Two-electrode cyclic voltammetry of the assembled PEC tandem device in 0.5 M H<sub>2</sub>SO<sub>4</sub> (photoanode as working electrode, photocathode as counter). The x-axis denotes the externally applied cell bias, where 0 V corresponds to unbiased operation.

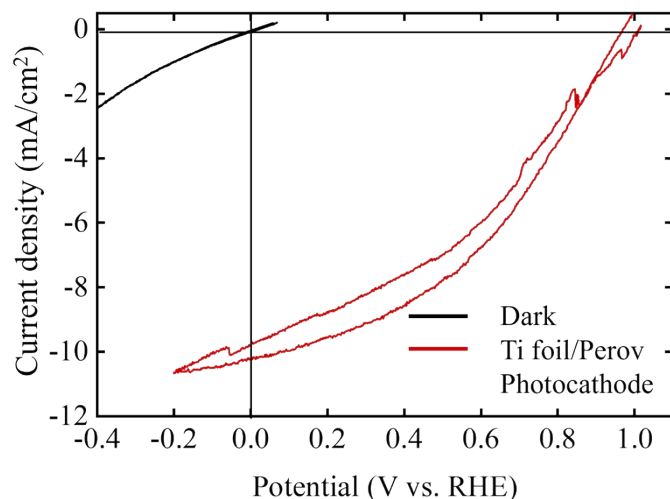


Figure S12. Three-electrode cyclic voltammetry of the halide perovskite photocathode on a titanium substrate in 0.5 M H<sub>2</sub>SO<sub>4</sub>, measured under illumination (red) and in the dark (black).

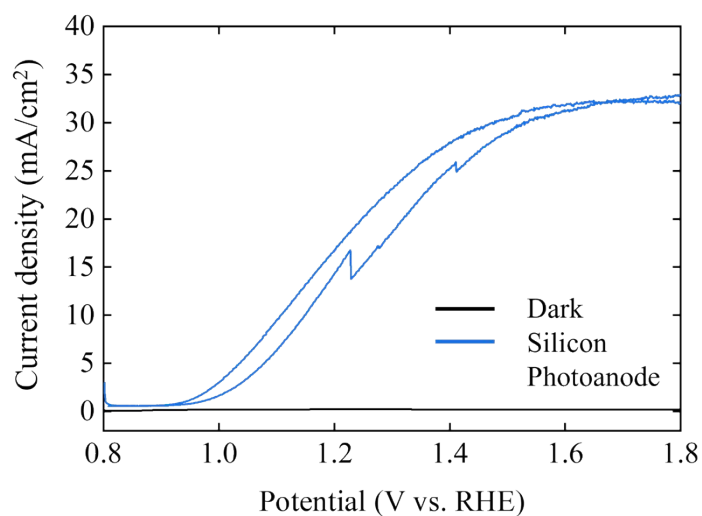


Figure S13. Three-electrode cyclic voltammetry of the silicon photoanode in 0.5 M  $\text{H}_2\text{SO}_4$ , with illumination incident through the single-crystal  $\text{TiO}_2$  protection layer (electrolyte-front). Blue: under illumination; black: dark.

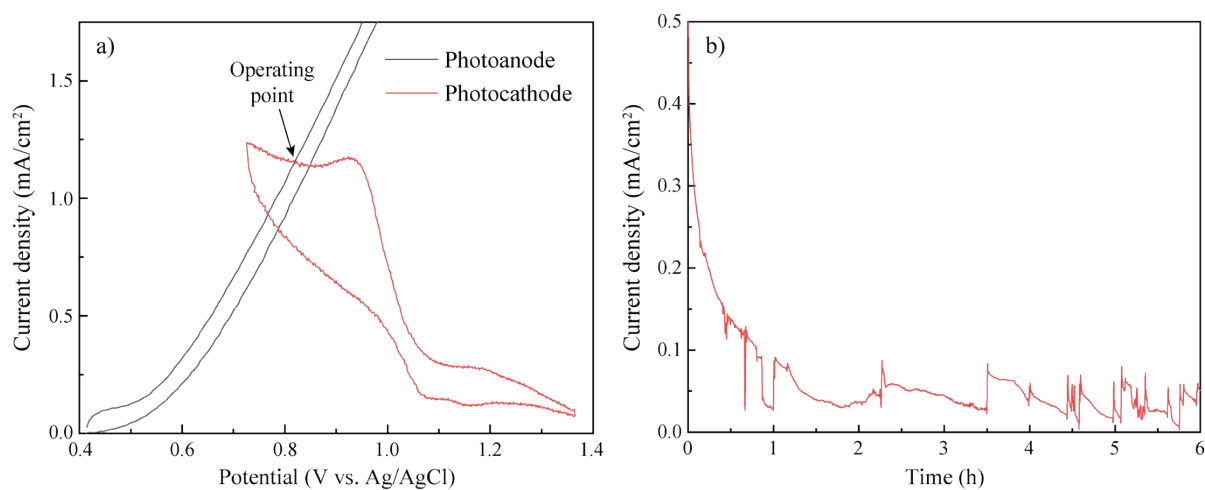


Figure S14. a) Overlap of cyclic voltammetric profiles of halide perovskite photocathode (black) and halide perovskite photoanodes (red). b) Chronoamperometric curves of parallel tandem device with a 2-electrode configuration.

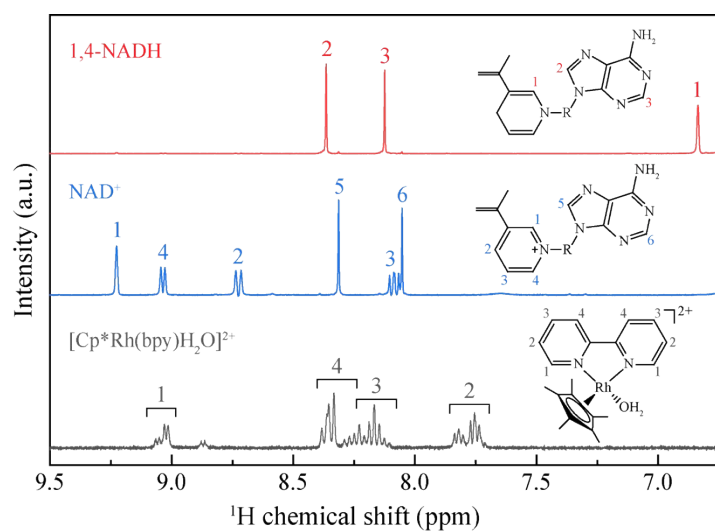


Figure S15.  $^1\text{H}$  NMR spectra of NADH,  $\text{NAD}^+$ , and  $\text{M}_{\text{ox}}$ . Solvent: a mixture of KPi buffer (100 mM, pH 7.5) and  $\text{D}_2\text{O}$  (volume ratio: 9/1).

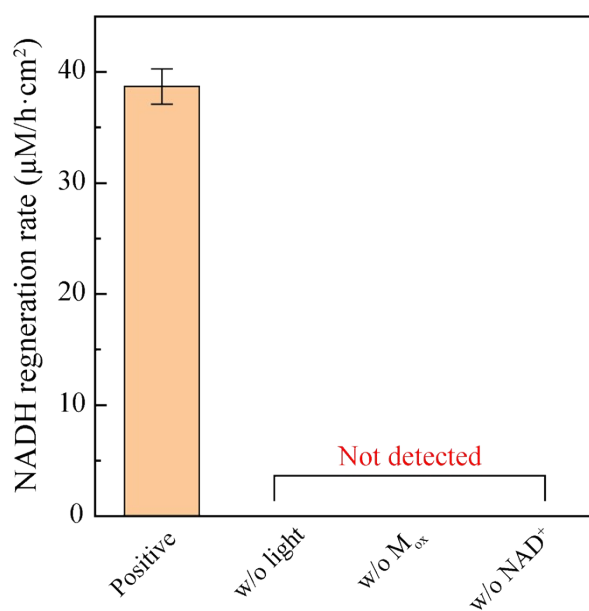


Figure S16. Control experiments of PEC regeneration of NADH from  $\text{NAD}^+$  using  $\text{TiO}_2$ -protected halide perovskite tandem device.



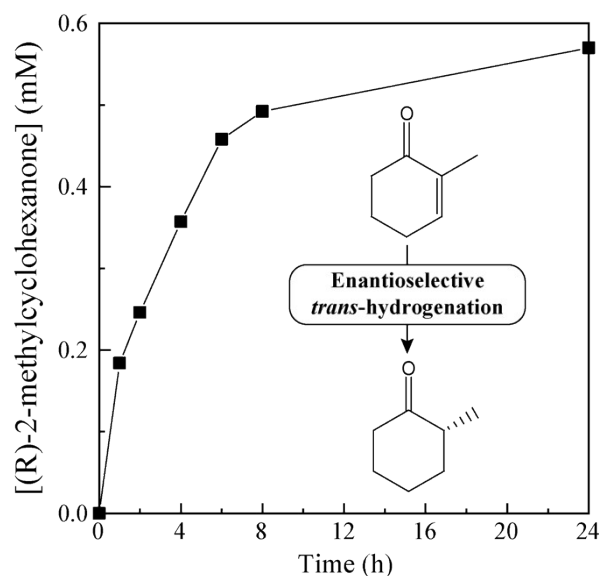


Figure S17. a) Time profiles of BPEC reaction in parallel tandem cell. Enzymatic substrate: 2-methyl-2-cyclohexen-1-one.

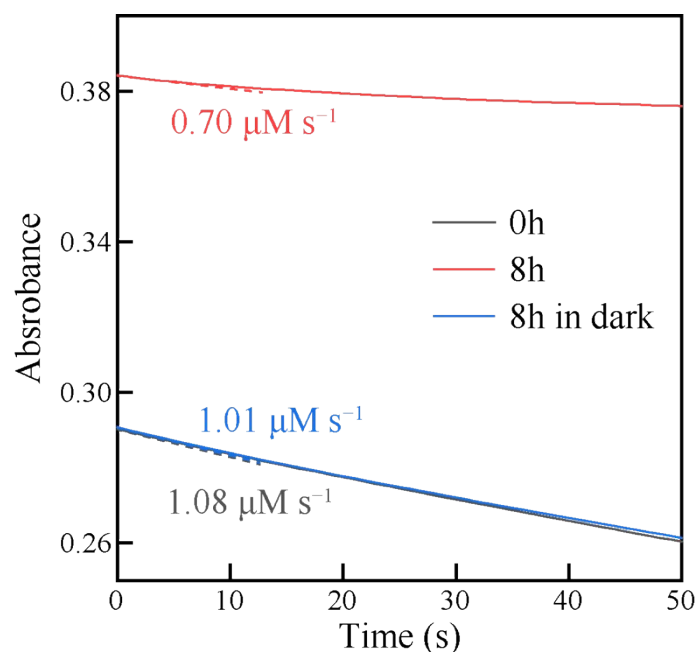


Figure S18. Change in initial activity of *TsOYE* after light illumination. We recorded time-dependent UV-Vis absorption spectra at 340 nm to monitor the consumption of NADH under light and dark conditions. The decrease in absorption at 340 nm originates from *TsOYE*-catalyzed oxidation of NADH to NAD<sup>+</sup>. The initial activity of *TsOYE* ( $\mu\text{M s}^{-1}$ ) was calculated from the initial slope of the curve. Light conditions: 1 sun illumination (AM 1.5 G, 100 mW cm<sup>-2</sup>).

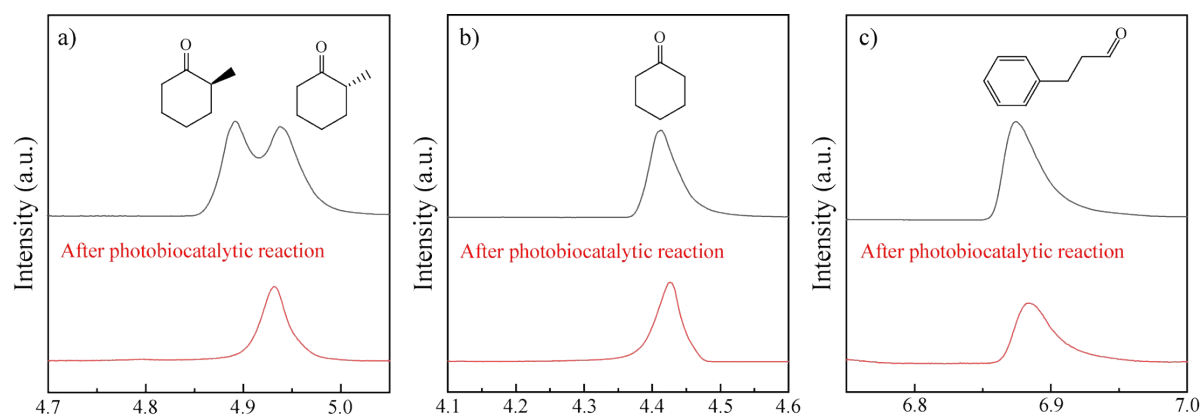


Figure S19. Gas chromatograms of enzymatic products. a) 2-Methylcyclohexanone. b) Cyclohexanone. c) 3-Phenylpropionaldehyde.

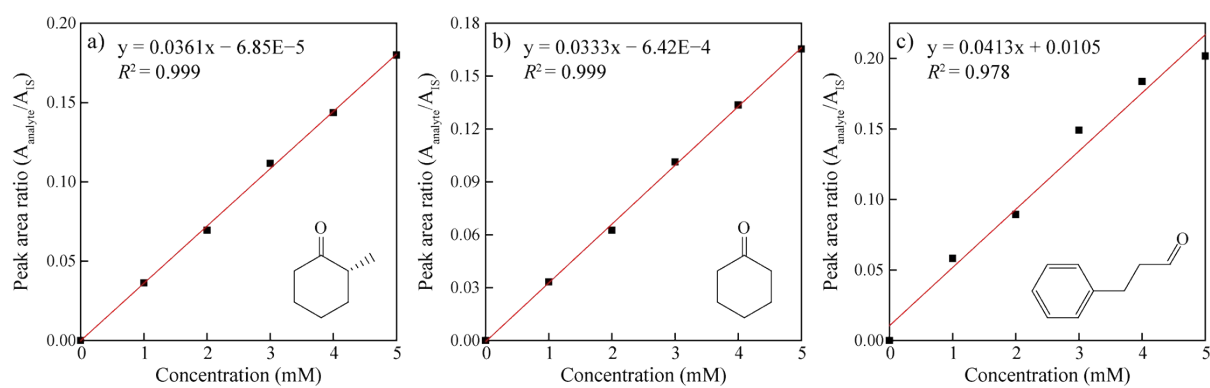


Figure S20. Calibration curves of enzymatic products using internal standard method. a) (*R*)-2-Methylcyclohexanone. b) Cyclohexanone. c) 3-Phenylpropionaldehyde.  $A_{\text{analyte}}$ : peak area of analyte.  $A_{\text{IS}}$ : peak area of internal standard.

Structure type	Stability assessment method	Type of electrolyte and stability test	Publication
TCO-front	ICP-OES	1M KOH (pH 14), operation over 43h	Nat. Energy, 2024, <b>9</b> , 272-284 Ref.[S1]
	CA	0.5 M H <sub>2</sub> SO <sub>4</sub> solution (pH 0.3-0.4), operation over 16.3h (t <sub>60</sub> )	Nat. Comm., 2023, <b>14</b> , 3797 Ref.[S2]
	CA	0.5 M KPi (pH 7), operation over 2h (t <sub>70</sub> )	Adv. Energy Mater., 2023, <b>13</b> , 2301693 Ref.[S3]
	CA	0.1M KPi solution (pH 7), operation over 6h	Nat. Comm., 2021, <b>12</b> , 1202 Ref.[S4]
	CA	0.5 M H <sub>2</sub> SO <sub>4</sub> solution, operation over 52h (t <sub>80</sub> )	Adv. Funct. Mater. 2021, <b>31</b> , 2008277 Ref.[S5]
	CA	0.5 M KHCO <sub>3</sub> solution (pH 7.2), operation over 34h (photoanode at 1.23V <sub>RHE</sub> )	Adv. Energy Mater. 2020, <b>10</b> , 2002105 Ref.[S6]
	CA	KOH solution (pH 12.5), operation over 34h	Nat.Comm., 2019, <b>10</b> , 2097 Ref.[S7]
	CA	0.1 M KPi (pH 7), operation over 3h (photocathode at 0 V <sub>RHE</sub> )	ACS Appl. Mater. Interfaces., 2019, <b>11</b> , 23198-23206 Ref.[S9]
	CA	1M HCl solution (pH 7), operation over 12h (t <sub>70</sub> )	ACS Appl. Energy Mater., 2019, <b>2</b> , 1969–1976 Ref.[S10]
<b>Electrolyte -front</b>	CA	0.5M H <sub>2</sub> SO <sub>4</sub> (pH 0.32), operation over 2h (t <sub>75</sub> )	ACS Energy Lett. 2019, <b>4</b> , 293–298 Ref.[S8]
	<b>ICP-MS</b>	<b>0.5M H<sub>2</sub>SO<sub>4</sub> solution (pH 0.3-0.4), operation over 12 hours</b>	<b>This work</b>

Table S1. Survey of long-term stability in halide-perovskite PEC devices by structure type, assessment method, and electrolyte: prior reports are largely TCO-front, which ease protection but suffer scale-dependent ohmic loss, while electrolyte-front examples are rare and short-live.

Elements	Cathode compartment (ppb)		Anode compartment (ppb)	
	Before test	After test	Before test	After test
Pb	4.02	3.49	2.08	5.20
Ti	11.6	22.3	7.34	43.4
Sn	8.38	323	1.19	94.5
Pt	3.27	5.43	0.112	1.13
Ir	0.959	89.0	0.231	975

Table S2. The concentration of elements in the electrolyte before and after the stability test (PEC water-splitting reaction for 12 hours). Two compartments are separated by a nafion membrane and the volume of each compartment is 3 ml. The detection limit of Pb, Ti, Sn, Pt and Ir are 0.02265, 0.7761, 0.02415, 0.009871, 0.005291 ppb, and the background equivalent concentration of the same elements are 0.0376, 0.3176, 0.01031, 0.0173, and 0.009385 ppb.

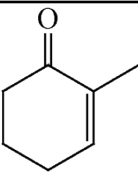
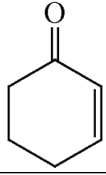
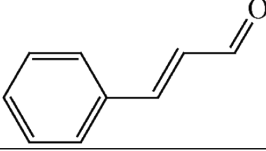
Substrate	Temperature profile	Retention time (min) <sup>[a]</sup>
	60 °C for 3 min, 20 °C min <sup>-1</sup> to 120 °C and hold for 4 min, 20 °C min <sup>-1</sup> to 180 °C and hold for 2 min	2-Methyl-2-cyclohexen-1-one: 5.1 ( <i>R</i> )-2-Methylcyclohexanone: 4.94 ( <i>S</i> )-2-Methylcyclohexanone: 4.89 1-Octanol: 6.23
	60 °C for 3 min, 20 °C min <sup>-1</sup> to 120 °C and hold for 4 min, 20 °C min <sup>-1</sup> to 180 °C and hold for 2 min	2-Cyclohexen-1-one: 4.62 Cyclohexanone: 4.42 1-Octanol: 6.23
	60 °C for 3 min, 20 °C min <sup>-1</sup> to 120 °C and hold for 4 min, 20 °C min <sup>-1</sup> to 180 °C and hold for 2 min	<i>trans</i> -3-Phenyl-2-propenal: 8.84 3-Phenylpropionaldehyde: 6.88 1-Octanol: 6.23
<sup>[a]</sup> 1-Octanol was used as an internal standard.		

Table S3. Gas chromatography oven programs for quantification of analytes.

Note S1. The equivalent thicknesses of ARC and catalysts dissolved during the water-splitting reaction are estimated by using the following equation.

$$t = \frac{(c_{cat}^{after} - c_{cat}^{before})V_{cat} + (c_{ano}^{after} - c_{ano}^{before})V_{ano}}{rAd}$$

Here,  $c_{cat}^{before}$ ,  $c_{cat}^{after}$ ,  $c_{ano}^{before}$ , and  $c_{ano}^{after}$  are the concentration of elements before and after the reaction in the cathodic and anodic compartments filled with electrolytes.  $V_{cat}$  and  $V_{ano}$  are the volume of the electrolytes in the cathodic and anodic compartments, which are both 3 ml.  $r$  is the atomic mass ratio between the element measured by ICP-MS and the unit cell of ARC or an electrocatalyst (e.g. For SnO<sub>2</sub>, 118.71/(118.71+2×16)).  $A$  is the surface area of the electrode, and  $d$  is the density of ARC or an electrocatalyst.

## Supplementary References

- 1 D. Hansora, J. W. Yoo, R. Mehrotra, W. J. Byun, D. Lim, Y. K. Kim, E. Noh, H. Lim, J.-W. Jang, S. Il Seok and J. S. Lee, *Nat. Energy*, 2024, **9**, 272–284.
- 2 A. M. K. Fehr, A. Agrawal, F. Mandani, C. L. Conrad, Q. Jiang, S. Y. Park, O. Alley, B. Li, S. Sidhik, I. Metcalf, C. Botello, J. L. Young, J. Even, J. C. Blancon, T. G. Deutsch, K. Zhu, S. Albrecht, F. M. Toma, M. Wong and A. D. Mohite, *Nat. Commun.*, 2023, **14**, 3797.
- 3 J. Yun, H. Lee, Y. S. Park, W. Jeong, C. Jeong, J. Lee, J. Lee, J. Tan, S. Ma, G. Jang, C. U. Lee, S. Moon, H. Im, S. Lee, D. Yee, J. Kim and J. Moon, *Adv. Energy Mater.*, DOI:10.1002/aenm.202301693.
- 4 X.-D. Wang, Y.-H. Huang, J.-F. Liao, Z.-F. Wei, W.-G. Li, Y.-F. Xu, H.-Y. Chen and D.-B. Kuang, *Nat. Commun.*, 2021, **12**, 1202.
- 5 J. Kim, S. Seo, J. Lee, H. Choi, S. Kim, G. Piao, Y. R. Kim, B. Park, J. Lee, Y. Jung, H. Park, S. Lee and K. Lee, *Adv. Funct. Mater.*, DOI:10.1002/adfm.202008277.

- 6 H. Zhang, Y. Chen, H. Wang, H. Wang, W. Ma, X. Zong and C. Li, *Adv. Energy Mater.*, DOI:10.1002/aenm.202002105.
- 7 I. Poli, U. Hintermair, M. Regue, S. Kumar, E. V. Sackville, J. Baker, T. M. Watson, S. Eslava and P. J. Cameron, *Nat. Commun.*, 2019, **10**, 2097.
- 8 S. Ahmad, A. Sadhanala, R. L. Z. Hoyer, V. Andrei, M. H. Modarres, B. Zhao, J. Rongé, R. Friend and M. De Volder, *ACS Appl. Mater. Interfaces*, 2019, **11**, 23198–23206.
- 9 R. Tao, Z. Sun, F. Li, W. Fang and L. Xu, *ACS Appl. Energy Mater.*, 2019, **2**, 1969–1976.
- 10 I. S. Kim, M. J. Pellin and A. B. F. Martinson, *ACS Energy Lett.*, 2019, **4**, 293–298.